Check for updates

Folate receptor-targeting mesoporous silica-coated gold nanorod nanoparticles for the synergistic photothermal therapy and chemotherapy of rheumatoid arthritis

Xiangyu Li, Yufei Hou, Xiangxue Meng, Ge Li, Fei Xu, Lesheng Teng, [ID] Fengying Sun* and Youxin Li [ID] *

The synergy of photothermal therapy (PTT) and chemotherapy is widely regarded as an effective treatment for complex diseases, such as cancer and inflammation. In this paper, we report the synthesis of a nanoscaled drug delivery system, which was composed of a gold nanorod (GNR) as the photothermal agent and a mesoporous silica shell as the methotrexate (MTX) reservoir, named FAGMs. Due to folate modification on the surface, FAGMs targeted specifically activated macrophages in rheumatoid arthritis (RA). Under 808 nm laser irradiation, FAGMs could kill macrophages by reaching sufficient local hyperthermia with excellent efficiency in the photothermal conversion of GNRs. Meanwhile, internal heating caused hydrogen bond fracture; thus, MTX released rapidly from FAGMs for localized synergistic PTT and chemotherapy. The FAGMs had a mean particle size of about 180 nm and a zeta potential of 14.36 mV. The release rate of MTX from FAGMs *in vitro* increased markedly under 808 nm laser irradiation. In a cellular uptake study, stronger fluorescence signals were observed in activated macrophages when treated with FAGMs, suggesting that folic acid molecules enabled the enhancement of endocytosis into activated macrophages. In rats with adjuvant-induced arthritis, synergistic treatment excellently inhibited the progression of RA. These results demonstrated that FAGMs could be promising for the treatment of RA.

Introduction

Rheumatoid arthritis (RA) is a chronic inflammatory disease with long-term psychological and physiological effects.[1] Its main clinical manifestations include severe synovial erosion, cartilage damage, and attendant psychological complications, such as depression and anxiety.[2–4] Although the pathogenesis of RA remains unknown, fibroblast-like synoviocytes, dendritic cells, macrophages and other immune cells have been verified to be deeply involved in the occurrence and development of RA.[5–8] Among these, activated macrophages have a non-negligible effect, mainly through two mechanisms.[9,10] First, activated macrophages express surface antigens, such as adhesion molecules, and secrete multiple chemokines, cytokines, growth factors, proteases and other mediators. These surface antigens and mediators facilitate the progression of RA by mediating inflammatory cell migration and neo-vascularization.[9,11,12] Second, synovial fibroblasts in RA might induce activated macrophages to differentiate into osteoclasts, causing severe cartilage damage.[13,14] Folate receptor β (FRβ) is

School of Life Sciences, Jilin University, 2699 Qianjin Street, Changchun, Jilin 130012, China. E-mail: sunfengying@jlu.edu.cn; liyouxin@jlu.edu.cn

a receptor overexpressed on the surface of RA-activated macrophages, which could specifically recognize and bind to a nanoscale drug delivery system modified with folic acid molecules (FA).[15,16] It was reported that this specific binding could mediate the cellular uptake of modified nanoparticles by activated macrophages,[17] which helped reduce the systemic toxicity and improve the effective concentration of chemotherapy drugs at the site of inflammation.

Methotrexate (MTX) has been widely used as the first-line chemotherapy drug for RA over last 40 years.[18–20] As an analogue of folic acid, MTX can effectively inhibit the proliferation of inflammatory cells.[21] Moreover, this drug also slows the progression of RA by reducing the accumulation of toxic metabolites and the intracellular level of glutathione.[22] With low cost and excellent efficacy, MTX has become the primary therapeutic drug for the clinical treatment of RA. However, the low bioavailability and systemic toxicity of MTX as a chemotherapeutic drug have limited its further application, and a safe and efficient delivery system is urgently needed.[23]

Compared to traditional radiotherapy, chemotherapy and operative therapy, photothermal therapy (PTT) shows higher biocompatibility and controllability due to its remote responsiveness and non-invasive properties.[24,25] One of the most

promising PTTs is the use of near-infrared (NIR) laser-triggered drug delivery systems. The advantage of NIR is that it has a super strong penetrability (centimetres) and causes less damage to the skin and tissue.[26] Gold nanostructures are considered safe, non-immunogenic and biocompatible NIR-responsive materials.[24] A variety of gold nanostructures have been used for NIR-responsive drug delivery systems, including gold nanorods (GNRs),[27] gold nanocages[28] and gold nanoshells.[29] GNRs as a typical material are attracting researchers' attention with their excellent photothermal conversion efficacy and tuneable longitudinal surface plasmon resonance (LSPR) wavelengths.[30] Nevertheless, GNRs still need to be prepared into hybrid nanoparticles with other biocompatible materials in order to solve their problem of a low drug loading capacity. Mesoporous silica nanoparticles (MSNs) have been widely used for drug delivery due to their controllable particle size and good biocompatibility. In particular, their large surface area and pore volume provide them with the potential for drug adsorption,[31] which make them suitable for the targeted delivery of MTX. The encapsulation of MTX is mainly achieved by adsorption into the mesopores of MSNs. Besides, FTIR analysis has enabled proving that MTX interacts with mesoporous silica by hydrogen bonding formed between MTX and silica.[32] Also, the weakly basic MTX attaches to the silanol bond on the mesoporous silica surface.[33,34] X-ray photoelectron spectroscopy (XPS) analysis has proven that MTX is not only adsorbed in the mesopores, but also attached on the external surface of MSNs.[35] With hexadecyl trimethyl ammonium bromide (CTAB) attached around the gold nanorods as a template, the mesoporous silicon layer could be easily coated on the surface of the gold nanorods.[30,36] Local hyperthermia caused by gold nanorods under NIR laser irradiation with chemotherapeutic drugs encapsulated inside the mesopores could be used for the synergistic treatment of RA.

Herein, we report a potential FA-modified targeted nanoscale drug delivery system named FAGMs. The internal GNR core and MTX encapsulated in silicon mesoporous endow the FAGMs with the ability to provide a synergistic treatment of PTT and chemotherapy for RA. The essential physico-chemical characteristics and FA-targeting properties of the FAGMs were confirmed in an *in vitro* study. The NIR-induced photothermal properties and NIR-triggered MTX release were evaluated under 808 nm laser irradiation. The therapeutic capacity *in vivo* of the FAGMs was performed in an adjuvant-induced arthritis (AIA) rat model.

Materials and methods

Materials

MTX, ascorbic acid, FA, *N*-hydroxysuccinimide (NHS), 1-ethyl-3-(3′-dimethylaminopropyl)carbodiimide (EDC) and $HAuCl_4$ were purchased from Shanghai Yuanye Bio-Technology Co., Ltd (Shanghai, China). Tetraethoxysilane (TEOS) and (3-aminopropyl) trimethoxysilane (APTES) were purchased from Sigma-Aldrich (St. Louis, MO, USA). H_2SO_4, N, *N*-dimethylformamide, citric acid and acetonitrile (DMF) were obtained from Beijing Chemical Works (Beijing, China). 4′,6-Diamidino-2-

phenylindole (DAPI) was purchased from Beyotime Institute of Biotechnology (Haimen, China). Fetal bovine serum (FBS) and RAW 264.7 cells were obtained from Wuhan Procell Biological Technology Co., Ltd (Wuhan, China). $NaBH_4$, $AgNO_3$, CTAB and complete Freund's adjuvant (CFA) were obtained from Shanghai Aladdin Bio-Chem Technology Co., LTD (Shanghai, China). Rat TNF-α ELISA kits and IL-6 ELISA kits were obtained from Elabscience Biotechnology Co., Ltd (Wuhan, China).

Synthesis of CTAB-coated GNRs (CTAB-GNRs)

GNRs were synthesized *via* the seed-mediated growth method. The gold seed solution was first synthesized by a chemical reduction of $HAuCl_4$ with $NaBH_4$. Briefly, 5 mL of 0.5 mM $HAuCl_4$ was mixed with 5 mL of 0.2 M CTAB, and then 0.6 mL of 0.01 M ice-cold $NaBH_4$ was injected into the above mixture quickly with vigorous stirring, and the colour of the mixed solution changed from light yellow to brown yellow immediately with the synthesis of the gold seed. After that, the gold seed solution was kept at 28 °C for further use.

Subsequently, the growth solution was prepared. CTAB (100 mL, 0.2 M), $HAuCl_4$ (100 mL, 1 mM), $AgNO_3$ (1 mL, 0.04 M) and H_2SO_4 (1 mL, 0.5 M) were mixed in a 250 mL breaker and kept at 28 °C with gentle stirring for 30 min. Afterwards, 1.4 mL of 0.0788 M ascorbic acid was injected into the above mixture drop by drop with vigorous stirring, and the solution changed from light yellow to colourless. Gold seed solution (240 μL) was added to the growth solution and kept at 28 °C overnight with gentle stirring for the growth of the GNRs.

Synthesis of mesoporous silica shell-coated GNRs (GMs)

To synthesize the GMs, 80 mL of as-synthesized CTAB-GNRs was centrifuged at 12 000 rpm for 15 min twice to remove excess CTAB, and then resuspended in 40 mL ultrapure water. The pH was adjusted to 10 with 0.1 M NaOH aqueous, and then the dispersion was incubated at 33 °C for 0.5 h. Subsequently, 1.8 mL of TEOS was injected into the dispersion as a silica source three times (0.6 mL per time) with gentle stirring at 30 min intervals. After gently stirring in the dark overnight, the GMs were collected by centrifugation at 12 000 rpm for 20 min and washed with methanol. To completely remove the residual CTAB in the mesopores, the obtained GMs were refluxed in a mixed solution (methanol : HCl = 16 : 1) at 80 °C for 12 h.

Synthesis of folic acid-functionalized GMs (FAGMs)

To graft an amino group on the nanoparticles, 100 μL of APTES was injected quickly into 40 mL ethanol suspension of the GMs. The suspension was stirred gently for 24 h at room temperature. Then, GMs-NH₂ was collected by centrifugation and washed three times with ethanol. The synthesis of FAGMs was performed using an EDC-NHS reaction. First, 20 mg folic acid (FA), 10 mg EDC and 8 mg NHS were dissolved in 20 mL anhydrous DMF, and incubated at room temperature overnight to activate the carboxyl groups of FA. Then, GMs-NH₂ (20 mg) was added. The mixed solution was allowed to react for 12 h, and the

FAGMs were obtained by centrifugation at 12 000 rpm for 20 min, and then washed with methanol three times.

Drug loading of MTX

MTX and FAGMs at the ratio of 1 : 1 (w/w) were dispersed in phosphate-buffered saline (PBS) solution under sonication. After 24 h of incubation, the MTX-loaded FAGMs (MTX-FAGMs) were obtained by centrifugation, and the supernatant containing free MTX was analyzed by reverse phase high-performance liquid chromatography (HPLC). The mobile phase consisted of acetonitrile, 2% Na_2HPO_4 solution and 7% citric acid solution in the ratio of 10 : 10 : 80 (v/v/v). The system was run at a flow rate of 1 mL min^{-1} and a temperature of 30 °C. The detection wavelength and injection volume were set at 302 nm and 20 μL, respectively. The drug loading (DL) of MTX in the nanoparticles was calculated using the following formula:

$$DL \text{ of } MTX(\%) = \frac{\text{amount of total MTX} - \text{amount of MTX in the supernatant}}{\text{amount of nanoparticles}} \times 100\%$$

Characterization

The size and zeta potential of GNRs, GMs, GMs-NH_2 and FAGMs were analyzed at 25 °C with a Malvern Zetasizer Nano ZS90. The nanoparticles were resuspended in deionized water to a concentration of 1 mg mL^{-1} before measurement. The morphology of GNRs and FAGMs was observed by transmission electron microscopy at a 200 kV accelerating voltage (H800, Hitachi, Japan). The UV-Vis-NIR spectra of GNRs and FAGMs were recorded with a spectrophotometer (UV-2700, Shimadzu, Japan). The specific surface area, pore volume and pore-size distributions were analyzed by nitrogen adsorption/desorption measurements.

Haemolysis assay

The biosafety and toxicity of an intravenous injection of FAGMs were detected using an haemolysis assay. Briefly, fresh whole blood collected from the orbits sinus of Sprague Dawley rats to isolate the red blood cells (RBCs) by centrifugation, and then the RBCs were diluted to 2% (v/v) with saline. FAGMs of different concentrations were suspended into 2% RBCs in 1.5 mL microtubes and then incubated at 37 °C for 3 h. Saline served as the negative control and 1% Triton X-100 served as the positive control. After centrifugation, the supernatants were transferred to 96-well plates, and the absorbance at 540 nm was obtained using a plate reader. The haemolysis rate was calculated using the following formula:

$$\text{Haemolysis ratio}(\%) = \frac{A_{\text{sample}} - A_{\text{negative control}}}{A_{\text{positive control}} - A_{\text{negative control}}} \times 100\%$$

In vitro NIR-induced photothermal assay and NIR-triggered MTX release

First, FAGMs (300 μL, 5 mg mL^{-1}) dispersed in water under sonication were injected into a 96-well plate, irradiated by the 808 nm NIR laser (MDL-III-808, Changchun New Industries Optoelectronics Technology Co., Ltd., China) at different power densities (0.5, 1.0 and 2.0 W cm^{-2}) for 8 min. Second, the FAGMs, folic acid-functionalized mesoporous silica nanoparticles (MSNs-FA) (300 μL, 5 mg mL^{-1}) suspension and equivalent CTAB-GNRs were injected into a 96-well plate, irradiated by the 808 nm NIR laser at 1.0 W cm^{-2} for 8 min, while water with the same irradiation was taken as a control. The temperature of the suspension was recorded with an infrared thermal camera (C2, Flir, USA).

To analyze the NIR-triggered release of MTX from FAGMs at different pH (7.4 and 4.5) PBS solution, 10 mg of MTX-FAGMs were suspended in 10 mL PBS solution with different pH values and transferred into dialysis bags. At a pre-specified interval, upon 5 min of 808 nm NIR laser irradiation, 4 mL of the supernatant was extracted and replaced with fresh buffer solution. The concentrations of MTX in the supernatant were analyzed by HPLC. Meanwhile, the release behaviour of MTX from the FAGMs in PBS at pH 7.4 and 4.5 without irradiation were investigated.

Cell culture

RAW 246.7 cells were incubated in Dulbecco's modified Eagle's medium (DMEM) containing 10% FBS at 37 °C in a humidified atmosphere of 5% CO_2.

Cellular uptake study

To verify the RA-targeting ability of FAGMs, activated RAW 264.7 cells induced by LPS were seeded in a 12-well plate. Then, FAGMs and GMs labelled with FITC were added at a concentration of 12.5 μg mL^{-1}. After 2 h of incubation, the cells were washed with PBS solution and fixed with 4% (w/v) formaldehyde for 20 min at 25 °C. Subsequently, the cellular nuclei were stained with DAPI. The internalization of nanoparticles by activated RAW 264.7 cells was observed by confocal laser scanning microscopy (CLSM) on an LSM710 system from Carl Zeiss Meditec (Jena, Germany).

Cytotoxicity study

To investigate the cytotoxicity of MTX-FAGMs, activated RAW 246.7 cells induced by LPS were treated with free MTX, MTX-FAGMs, MTX-FAGM with 808 nm NIR laser irradiation, MTX-GMs and MTX-GMs with 808 nm NIR laser irradiation at a series of MTX concentrations (0.1, 1, 10 and 100 μg mL^{-1}). The power density and irradiation time of the NIR laser were 1.0 W cm^{-2} and 5 min, respectively. The cell viability was obtained by MTT assay and calculated using the following formula:

$$\text{Cell viability} = \frac{A_{\text{sample}} - A_{\text{blank}}}{A_{\text{negative control}} - A_{\text{blank}}} \times 100\%.$$

In addition, an MTT assay was conducted to evaluate the photothermal effect of MSNs-FA and blank FAGMs without MTX on activated macrophages. Briefly, activated RAW 246.7 cells induced by LPS were treated with MSNs-FA and FAGMs with 808 nm NIR laser irradiation (1.0 W cm^{-2}, 5 min) at a series of concentrations (0.1, 1, 10 and 100 μg mL^{-1}). The cell viability was calculated as mentioned above.

In vivo therapeutic efficacy

Male Sprague Dawley rats (160–180 g) were obtained from the Experimental Animal Center of Jilin University. All animal procedures were performed in accordance with the Guidelines for Care and Use of Laboratory Animals of Jilin University and all experiments were approved by the Institutional Animal Care and Use Committee of Jilin University. An AIA rat model was established by subcutaneously injecting 50 μL of CFA at the left footpad of the rats.

On day 14 after the CFA induction, the rats were randomly divided into five groups: MTX-FAGMs with laser, MTX-FAGMs, MTX-GMs, free MTX and control group, respectively. MTX-FAGMs, MTX-GMs or free MTX were administered by intravenous injection every two days for a total of six times, and rats treated with the same volume of saline served as a control group. Then, 30 min after each treatment, the inflammatory site of the rats from the MTX-FAGMs with the laser group was exposed to the 808 nm NIR laser at 1.0 W cm^{-2} for 5 min. The clinical scores of the joint swelling severity and thickness of the hind paws were recorded daily for each rat after the initiation of treatment.

Histological analysis

All the rats were euthanized on day 24. Then the ankle joints were obtained and fixed in 4% formaldehyde for one day. After a month of decalcification, the ankle joints were stained with haematoxylin and eosin (H&E) and observed using an Olympus microscope (Olympus, Tokyo, Japan).

Cytokine assay

On day 24 after the CFA treatment, serum was obtained by centrifugation of fresh whole blood collected from the experimental rats. The serum concentrations of TNF-α and IL-6 were determined using ELISA kits.

Statistical analysis

These data are expressed as the mean ± standard deviation (SD). Statistical analysis was performed using GraphPad Prism 8. Origin 2020 was used to compare the mean values. Group statistical significance was measured using one-way analysis of variance. Statistical significance was assigned as *$p < 0.05$, **$p < 0.01$ and ***$p < 0.001$. $P < 0.05$ was considered to indicate statistically significant differences.

Results

Synthesis and characterization of the FAGMs

The synthesis of FAGMs included the following steps: synthesis of GNRs, coating of mesoporous silicon shells on GNRs and grafting of FA on the surface of GMs. The TEM results (Fig. 1A and B) showed that the mesopores silicon layer with a thickness of about 20 nm was successfully coated on the surface of the rod-like GNRs by using the cationic surfactant CTAB as a template. Fig. 1C shows that the GNRs had an LSPR wavelength of 808 nm and a transverse surface plasmon resonance (TSPR) wavelength of 520 nm. Due to the presence of the mesoporous SiO$_2$ layer, the LSPR of GMs exhibited a red-shift of 25 nm. The synthesis steps of FAGMs were accompanied by a significant changes in the particle size and zeta potential of the nanoparticles, which could be observed in Fig. 1D.

As shown in Fig. 2A, B and C, the mesoporous pore size, surface area and BJH pore volume of the GMs were 3.4 nm, 1097.09 m^2 g^{-1} and 1.30 cm^3 g^{-1}, respectively, while those of the FAGMs were 3.1 nm, 978.50 m^2 g^{-1} and 1.12 cm^3 g^{-1}, respectively. All these ensured the drug-loading capacity of the nanoparticles. The DL of MTX was 27.58%.

Haemolysis assay

An haemolysis assay was performed to confirm the biosafety of the FAGMs. Fig. 2D shows that no visible haemolysis was observed within the FAGMs concentration of 1.56–100 μg mL^{-1}. This result guarantees the biosafety of the FAGMs for use *in vivo* by intravenous injection.

In vitro photothermal property and NIR-triggered drug release

Fig. 3A shows that the power density affected the photothermal efficiency of the FAGMs. The temperature of the FAGMs suspension was raised slowly ($\Delta T = 20.23$ °C) under an 808 nm NIR laser at 0.5 W cm^{-2}, but increased quickly at 1.0 and 2.0 W cm^{-2} ($\Delta T = 39.47$ °C, 48.40 °C, respectively). A high-intensity laser may injure the normal tissues and bring pain to
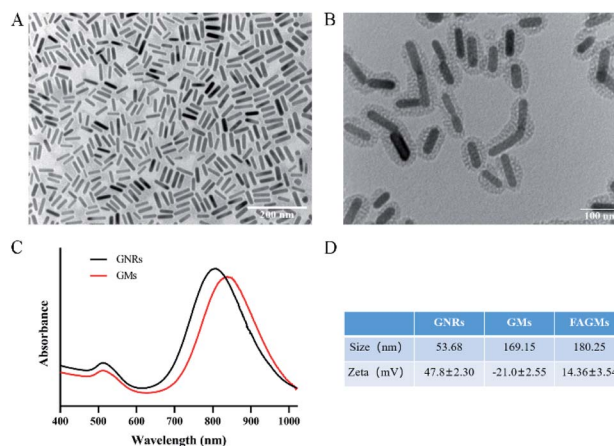

Fig. 1 TEM images of GNRs (scale bar, 200 nm) (A) and FAGMs (scale bar, 100 nm) (B). (C) UV-vis-NIR absorbance spectra of GNRs and GMs. (D) Particle size and zeta potential of GNRs, GMs and FAGMs.
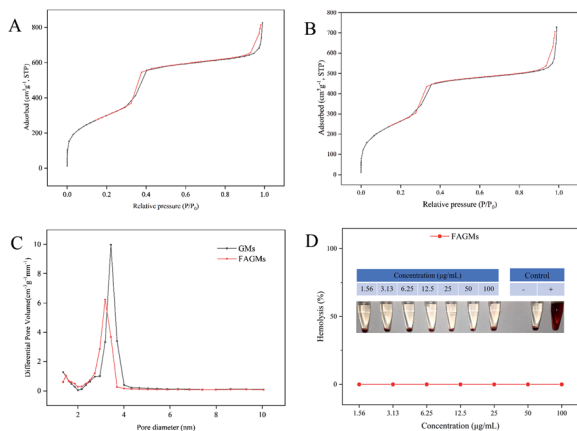
Fig. 2 Nitrogen sorption isotherm of GMs (A) and FAGMs (B). (C) The pore-size distribution of GMs and FAGMs. (D) Haemolysis assay of FAGMs.
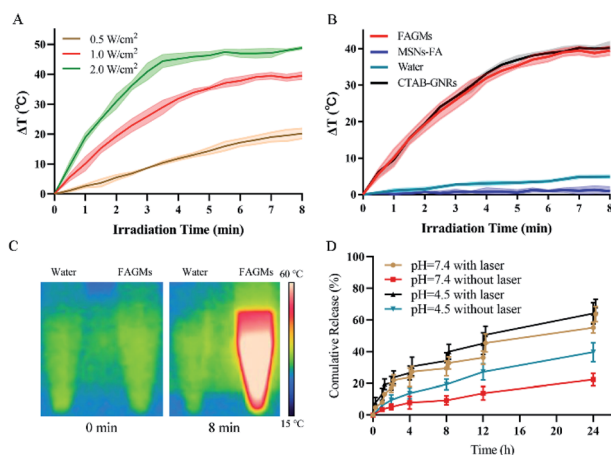

Fig. 3 (A) NIR-induced heating profiles of FAGMs under 808 nm NIR laser irradiation at the following power densities: 0.5, 1.0, 2.0 W cm^{-2} (B) NIR-induced heating profiles of FAGMs, MSNs-FA, water and CTAB-GNRs under 808 nm NIR laser irradiation at 1.0 W cm^{-2}. (C) The infrared thermal images of water and FAGMs. (D) *In vitro* release of MTX from FAGMs at different pH and NIR laser irradiation on/off cycles.

patients. Considering the patient's tolerance and safety, 1.0 W cm^{-2} was selected for further use.

As shown in Fig. 3B and C, the temperatures of the FAGMs and CTAB-GNRs suspension were recorded with similar heating profiles under an 808 nm NIR laser at 1.0 W cm^{-2}. In contrast, the temperatures of water and MSNs-FA suspension hardly increased (ΔT = 4.93 °C, 0.97 °C, respectively). These results suggested that the folic acid-functionalized mesoporous silica shell had no effect on the photothermal properties of the GNRs. Both the FAGMs and CTAB-GNRs showed excellent photothermal conversion efficacy. Also, the pure MSNs-FA without the GNR core showed no photothermal effect.

Local hyperthermia caused by NIR laser accelerated the release of MTX from the FAGMs by disrupting the hydrogen bonds between MTX and the mesoporous surface. Fig. 3D shows that the MTX-FAGMs at pH 7.4 and 4.5 were released

rapidly under NIR laser irradiation on/off cycles, with up to 63.74% and 68.75% cumulative release, respectively. For comparison, the cumulative release amounts without NIR laser irradiation were 22.38% and 39.69%, respectively. It is noteworthy that once the NIR laser was switched off, the release rate of MTX could be observed to decrease significantly. Meanwhile, these results confirmed that the acidic microenvironment of the inflammation site could also disrupt the hydrogen bonds, thereby accelerating the release of MTX.

Cellular uptake study

To evaluate the targeting and internalization behaviour of the FA-modified nanoparticles toward activated macrophages, a cell uptake study was performed. As shown in Fig. 4A, after incubation with FITC-labelled FAGMs and GMs, almost no FITC fluorescence was observed in non-activated RAW 264.7 cells, while a low FITC fluorescence density was observed around the nucleus of the activated RAW 264.7 cells treated with FITC-labelled GMs. Meanwhile, a strong fluorescence intensity of FITC was observed in activated RAW 264.7 cells treated with FITC-labelled FAGMs. Activated RAW 264.7 cells treated with FITC-labelled FAGMs showed a significant signal enhancement, compared with the other treatment groups (Fig. 4B). These results indicated that the modification of FA on the surface of GMs could give nanoparticles the ability to target activated macrophages and help the internalization of nanoparticles by activated RAW 264.7 cells.

Cytotoxicity

The cytotoxicity of MTX-FAGMs on activated macrophages was evaluated by MTT assay. Fig. 4C shows that all the experimental groups exhibited a concentration-dependent cytotoxicity. The free MTX-treatment group at all concentrations had the lowest cytotoxicity to macrophages. MTX-FAGMs, MTX-GMs with laser, while the MTX-GMs-treatment groups at 100 μg mL^{-1} MTX concentration showed a similar cytotoxicity, and the MTX-FAGMs with laser-treatment group exhibited a significantly higher cytotoxicity (a cell survival rate of 24.5%). These results could be attributed to the synergistic effect of PTT and chemotherapy under NIR laser irradiation.
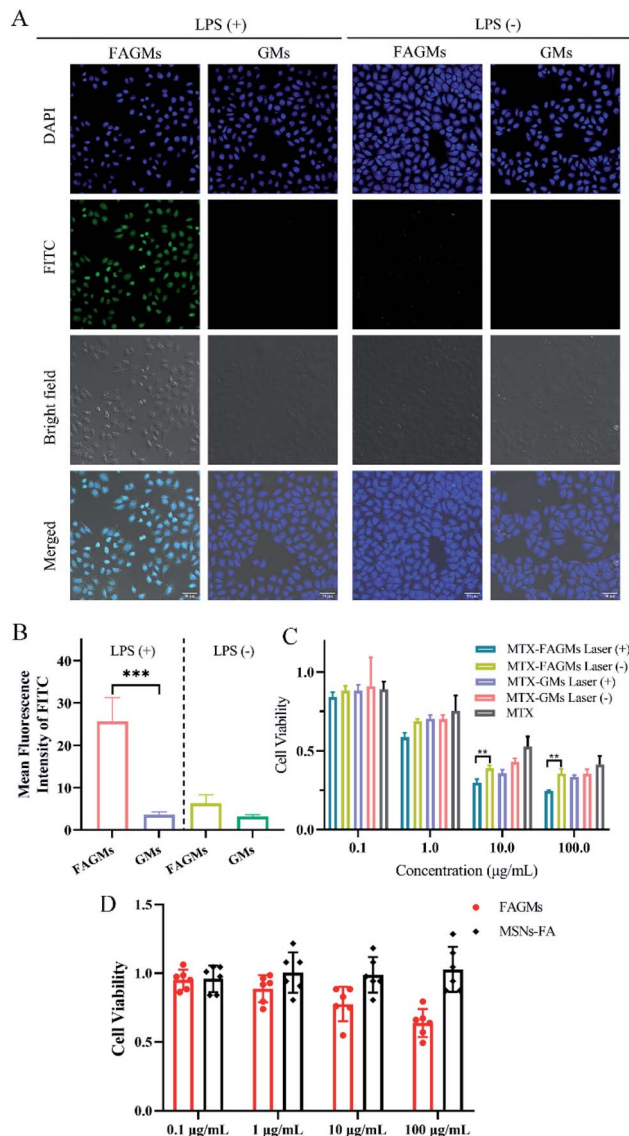
As shown in Fig. 4D, upon 5 min 808 nm NIR laser irradiation at 1.0 W cm^{-2}, the MSNs-FA without the GNR core exhibited no photothermal cytotoxicity on activated RAW 264.7 cells at concentrations between 0.1–100 μg mL^{-1}. The blank FAGMs without MTX exhibited a concentration-dependent cytotoxicity on activated macrophages under NIR laser irradiation. These above results help us understand the different roles and synergy of PTT and chemotherapy.

***In vivo* RA therapy**

The anti-inflammatory effect of the prepared nanoparticles was verified by clinical score, using the paw thickness as the evaluation method.
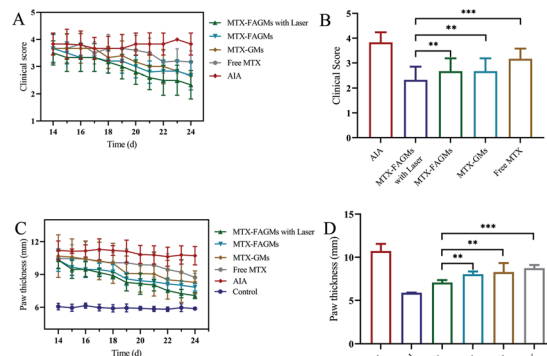
As shown in Fig. 6A, serious swelling and erythema were observed in the left hind paws of the AIA rats. After treatment with the different formulations encapsulated with MTX or free
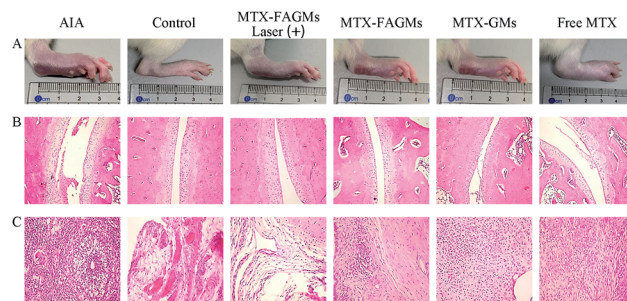
Fig. 4 (A) Uptake of RAW 264.7 cells after activation by LPS (+) or not (−) incubated with FITC-labelled FAGMs and GMs. (Scale bar, 50 μm). (B) Corresponding mean fluorescence intensity of RAW 264.7 cells after activation by LPS (+) or not (−) incubated with FITC-labelled FAGMs and GMs. (C) Cell viability of activated macrophages treated with free MTX, MTX-FAGMs, MTX-FAGM with laser, MTX-GMs and MTX-GMs with laser at a series of MTX concentrations. (D) Cell viability of activated macrophages treated with FAGMs and MSNs-FA at different concentrations under NIR laser irradiation.

Fig. 5 Therapeutic efficacy treated with MTX-FAGMs with laser, MTX-FAGMs, MTX-GMs and free MTX in AIA rats. (A) Clinical score change after treatment, (B) clinical score on day 24, (C) paw thickness change after treatment and (D) paw thickness on day 24 of the rats in each group.

Fig. 6 Photographs of the hind paws (A), H&E staining of the ankle joint (B) and periarticular soft tissues (C) of the rats in each group.
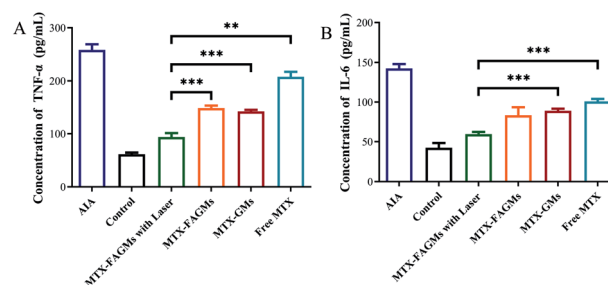

Fig. 7 Serum concentrations of TNF-α (A) and IL-6 (B).

MTX, the swelling began to ameliorate gradually in all the treatment groups (Fig. 5A). It is worth noting that the clinical score (2.33) of the MTX-FAGMs with laser-treatment group on day 24 was significantly lower than those of the other treatment groups (Fig. 5B). Meanwhile, the paw thickness measured by callipers decreased from day 15. The rats from MTX-FAGMs with the laser-treatment group were observed to show a faster decline in paw thickness than those of the other groups (Fig. 5C), which were closest to the control group on day 24 (Fig. 5D). All these results suggested that MTX-FAGMs with NIR

laser irradiation possessed an excellent synergistic anti-inflammatory effect for RA therapy.

Histological analysis

HE staining of the ankle joints was conducted to further verify the therapeutic effect of the various formulations on the histological level (Fig. 6B and C). The AIA rats treated with normal saline displayed severe inflammatory cell infiltration and cartilage damage. Relative relief was observed in AIA rats treated with MTX-FAGMs, MTX-GMs and free MTX, but still had

varying degrees of symptoms. Satisfactorily, the rats from MTX-FAGMs with laser-treatment group had only minimal infiltration of inflammatory cells, and the cartilage surfaces were almost alleviated to normal levels.

Cytokine assay

Activated macrophages promote the further deterioration of RA by secreting pro-inflammatory cytokines. Naturally, the serum level of IL-6 and TNF-α could serve as an evaluation standard for treatment effects. Compared with the control group, the serum levels of pro-inflammatory cytokines in AIA rats increased significantly. After treatment with various formulations, varying degrees of decline in inflammatory factor levels were observed. Fig. 7A and B show that the AIA rats treated with MTX-FAGMs with laser treatment had the lowest serum level of IL-6 and TNF-α, which were close to the control group.

Conclusions

In summary, we prepared nanoscale MTX-FAGMs, and verified their specific targeting cytotoxicity to activated macrophages under NIR laser irradiation for the treatment of RA. The obtained FAGMs had a typical morphology and particle size with a uniform size distribution. The excellent pore size, surface area and BJH pore volume provided a high MTX loading capacity for FAGMs. Interestingly, the MTX encapsulated in FAGMs showed accelerated release under the acidic microenvironment of macrophages and the local hyperthermia caused by NIR laser irradiation ensured the synergistic effect of nanoparticle PTT and chemotherapy, which was confirmed by the results of a cytotoxicity study and the *in vivo* anti-inflammatory treatment study.

A series of syndromes brought about by RA can seriously damage the physical and mental health of patients and their families. The use of targeted MTX-FAGMs, combined NIR-induced PTT and traditional chemotherapy could inhibit the progression of RA and reduce the systemic toxicity of MTX. It is thus considered to be a desirable nanodrug delivery platform for the treatment of RA.

Conflicts of interest

There are no conflicts to declare.

Acknowledgements

Notes and references

1 A. C. Boer, T. W. J. Huizinga and M. van der Helm-van, *Ann. Rheum. Dis.*, 2019, **78**, 2.

2 S. J. Chen, G. J. Lin, J. W. Chen, K. C. Wang, C. H. Tien, C. F. Hu, C. N. Chang, W. F. Hsu, H. C. Fan and H. K. Sytwu, *Int. J. Mol. Sci.*, 2019, **20**, 23.

3 M. Ribon, S. Seninet, J. Mussard, M. Sebbag, C. Clavel, G. Serre, M. C. Boissier, L. Semerano and P. Decker, *J. Autoimmun.c*, 2019, **98**, 122–131.

4 F. Rivellese, A. Lobasso, L. Barbieri, B. Liccardo, A. de Paulis and F. W. Rossi, *Curr. Med. Chem.*, 2019, **26**, 2823–2843.

5 C. Mauri and M. R. Ehrenstein, *Arthritis Res. Ther.*, 2007, **9**, 6.

6 A. P. Simopoulos, *Exp. Biol. Med.*, 2008, **233**, 674–688.

7 I. B. McInnes and G. Schett, *N. Engl. J. Med.*, 2011, **365**, 2205–2219.

8 Y. Y. Liu, S. Y. Wang, Y. N. Li, W. J. Bian, L. Q. Zhang, Y. H. Li, L. Long, X. Liu, X. W. Zhang and Z. G. Li, *Chin. Med. J.*, 2020, **6**, 679–686.

9 Y. Y. Ma and R. M. Pope, *Curr. Pharm. Des.*, 2005, **11**, 569–580.

10 R. W. Kinne, B. Stuhlmüller and G. R. Burmester, *Arthritis Res. Ther.*, 2007, **9**, 224.

11 Z. Szekanecz and A. E. Koch, *Curr. Opin. Rheumatol.*, 2007, **19**, 289–295.

12 M. Wahle and C. G. O. Baerwald, *Internist*, 1999, **40**, 930–935.

13 H. Takayanagi, H. Oda, S. Yamamoto, H. Kawaguchi, S. Tanaka, T. Nishikawa and Y. Koshihara, *Biochem. Biophys. Res. Commun.*, 1997, **240**, 279–286.

14 M. K. Neog and M. Rasool, *Eur. J. Pharm. Biopharm.*, 2018, **133**, 162–175.

15 P. K. Pandey, R. Maheshwari, N. Raval, P. Gondaliya, K. Kalia and R. K. Tekade, *J. Colloid Interface Sci.*, 2019, **544**, 61–77.

16 P. S. Low, W. A. Henne and D. D. Doorneweerd, *Acc. Chem. Res.*, 2008, **41**, 120–129.

17 M. D. Yang, J. X. Ding, Y. Zhang, F. Chang, J. C. Wang, Z. L. Gao, X. L. Zhuang and X. S. Chen, *J. Mater. Chem. B*, 2016, **4**, 2102–2113.

18 P. E. Lipsky, D. M. van der Heijde, E. W. St Clair, D. E. Furst, F. C. Breedveld, J. R. Kalden, J. S. Smolen, M. Weisman, P. Emery, M. Feldmann, G. R. Harriman and R. N. Maini, *N. Engl. J. Med.*, 2000, **343**, 1594–1602.

19 B. Friedman and B. Cronstein, *Jt., Bone, Spine*, 2019, **86**, 301–307.

20 M. Abbasi, M. J. Mousavi, S. Jamalzehi, R. Alimohammadi, M. H. Bezvan, H. Mohammadi and S. Aslani, *J. Cell. Physiol.*, 2019, **234**, 10018–10031.

21 S. Ramiro, A. Sepriano, K. Chatzidionysiou, J. L. Nam, J. S. Smolen, D. van der Heijde, M. Dougados, R. van Vollenhoven, J. W. Bijlsma, G. R. Burmester, M. Scholte-Voshaar, L. Falzon and R. B. M. Landewe, *Ann. Rheum. Dis.*, 2017, **76**, 1093–1101.

22 J. Pope, E. Keystone, S. Jamal, L. Wang, L. Fallon, J. Woolcott, I. Lazariciu and B. Haraoui, *Arthritis Rheumatol.*, 2016, **68**, 2.

23 G. Choi, T. H. Kim, J. M. Oh and J. H. Choy, *Coord. Chem. Rev.*, 2018, **359**, 32–51.

24 B. P. Timko, T. Dvir and D. S. Kohane, *Adv. Mater.*, 2010, **22**, 4925–4943.

25 T. Okuno, S. Kato, Y. Hatakeyama, J. Okajima, S. Maruyama, M. Sakamoto, S. Mori and T. Kodama, *J. Controlled Release*, 2013, **172**, 879–884.

26 V. Ntziachristos, J. Ripoll, L. H. V. Wang and R. Weissleder, *Nat. Biotechnol.*, 2005, **23**, 313–320.

27 Y. Q. Zhao, Y. Sun, Y. Zhang, X. Ding, N. Zhao, B. Yu, H. Zhao, S. Duan and F. J. Xu, *ACS Nano*, 2020, **14**, 2265–2275.

28 M. S. Yavuz, Y. Y. Cheng, J. Y. Chen, C. M. Cobley, Q. Zhang, M. Rycenga, J. W. Xie, C. Kim, K. H. Song, A. G. Schwartz, L. H. V. Wang and Y. N. Xia, *Nat. Mater.*, 2009, **8**, 935–939.

29 P. K. Jain, K. S. Lee, I. H. El-Sayed and M. A. El-Sayed, *J. Phys. Chem. B*, 2006, **110**, 7238–7248.

30 P. Blaszkiewicz, M. Kotkowiak, E. Coy and A. Dudkowiak, *J. Phys. Chem. C*, 2020, **124**, 2088–2095.

31 Y. Wang, Q. Zhao, N. Han, L. Bai, J. Li, J. Liu, E. Che, L. Hu, Q. Zhang, T. Jiang and S. Wang, *Nanomedicine*, 2015, **11**, 313–327.

32 M. Trukawka, K. Cendrowski, W. Konicki and E. Mijowska, *Appl. Sci.*, 2020, **10**, 6465.

33 A. Wani, G. H. L. Savithra, A. Abyad, S. Kanvinde, J. Li, S. Brock and D. Oupický, *Sci. Rep.*, 2017, **7**, 2274.

34 S. Sapino, S. Oliaro-Bosso, D. Zonari, A. Zattoni and E. Ugazio, *Int. J. Pharm.*, 2017, **530**, 239–248.

35 L. B. d. O. Freitas, I. J. G. Bravo, W. A. d. A. Macedo and E. M. B. de Sousa, *J. Sol-Gel Sci. Technol.*, 2016, **77**, 186–204.

36 J. Liu, C. Detrembleur, M. C. De Pauw-Gillet, S. Mornet, C. Jerome and E. Duguet, *Small*, 2015, **11**, 2323–2332.

© 2021 The Author(s). Published by the Royal Society of Chemistry